IPP-Report

Max-Planck-Institut für Plasmaphysik

Jakob Brenner

Purely ECR-heated H-modes in ASDEX Upgrade -
modeling with TGLF the effect of EC deposition on central ion temperature

IPP 2020-12
November 2020

Purely ECR-heated H-modes in ASDEX Upgrade -

modeling with TGLF the effect of EC deposition on central ion temperature

Report based on the bachelor thesis handed in at the LMU Munich on 3.2.2020

By Jakob Brenner

Contents

1 Introduction: Motivation & Aims

The physics of fusion plasmas has been a topic of research for quite some time and is certain to still produce a lot of interest in the future as it offers a near limitless capacity for energy production.

In current tokamaks the plasma heating processes are dominated by neutral beam injection systems. These systems deposit a large fraction of their power in the ion component, and are very versatile. [1]

This dominance of Ion heating however is subject to change. For future projects and power producing reactors like ITER an increasing fraction of the heating power will be deposited into the electrons instead of the ions, because of the higher beam energy of the new NBI systems, the reliance on ECR-heating and the heating through α-particles.

ECR (Electron Cyclotron Resonance)-heating is being increased due to its high flexibility (e.g. localized current drive or mode stabilization) and its small port requirements.

ECRH is also very attractive for stellarator experiments as it has additional utility like the ability to to compensate bootstrap currents. The stellarator W7X in Greifswald is using ECRH as the main heating system. [2]

A recent survey of ion temperature profiles in ECRH dominated W7-X plasmas [3] shows that no strong dependence of the central ion temperature on either the electron temperature or the ion density exists, meaning that higher central heat deposition has only very little impact on the ion temperature. The ion heating, which occurs through heat transport from the electrons, influences in these cases the profile very little which suggests the existence of a critical ion temperature gradient which cannot be exceeded under typical conditions.Higher temperatures were only achieved in higher density phases after pellet injections.[3] [4]

These findings resemble observations in a tokamak. Since in a tokamak transport is typically well described with the trapped gyro Landau fluid (TGLF), the modeling of such a case is planned for this thesis. In order to further challenge this transport model it is used to model a strong variation of the EC deposition profile. EC power shall be moved stepwise from the core to the pedestal top. Since in a tokamak transport is typically well described with the trapped gyro Landau fluid (TGLF), the modeling of such a case is planned for this thesis. In order to further challenge this transport model it is used to model a strong variation of the EC deposition profile. EC power

shall be moved stepwise from the core to the pedestal top..

The ASTRA model is an iterative simulation starting from experimental data and using the TGLF code to continually update the differing fluxes while holding a boundary condition fixed to the starting conditions. The used model is discussed in Section 2.

The chosen experiment is a density regime in which the temperatures at the boundary have almost equilibrated but in the center it is still possible for them to diverge (with T_e T_i. In the case of a stiff profile this is important as this allows constant boundary conditions invariant of the heating profile, which is facilitates the comparison the different simulations.

2 Methods & Background

2.1 ASDEX-Upgrade

ASDEX Upgrade (derived from Axial Symmetric Divertor EXperiment) is a tokamak experiment located in Garching close to Munich and run by the Max Planck Institute for Plasma Physics.

The simulation is based on an experiment that was using this tokamak.

ASDEX Upgrade is a mid-size experiment with a major radius of the plasma of 1.65 m and an aspect ratio of 3.2. It allows for pulses of a duration shorter than 10 seconds with total heating power of up to 27 MW, with the dominant mechanism being the NBI heating. The plasma chamber has a minor horizontal radius of 0.5 m with an ellipticity of up to 1.8.

Currently the ECRH system of ASDEX-Upgrade consists of 8 gyrotrons with a total ECRH power of up to 8 MW for up to 10 s, working at 105 and 140 GHz.

Most of the data used in my simulation was derived from the higher level diagnostics IDA (Integrated Data Analysis) or IDI, the equivalent for ions. These diagnostics combine several basic diagnostics and use Bayesian statistics [5] to produce the final output.

IDI provides the ion temperature and the toroidal angular velocity as well as different gradients. All available data among the diagnostics CEZ, COZ, CUZ and CMZ is used.

IDA provides data for: the electron density, electron temperature and electron pressure and their gradients. The base diagnostics used are DCN interferometry (DCK or DCN) and ECE (CEC). Additionally the diagnostic uses data from LIB (lithium beam emission data). [5]

CEZ is the charge exchange recombination spectroscopy. This diagnostic measures the radiation spectrum produced by impurity ions in the plasma which are excited by charge exchange reaction with fast neutral atoms. This is convenient as the plasma is optically thin in that spectral range. [6] The other diagnostics (COZ, CUZ and CMZ) are names for diagnostics using the same principle at different positions and with different lines of sight. IDI unites these diagnostics into as single data set.

The DCN is an interferometric measurement of electron density or rather the phase shift of light due to the electron density. For this diagnostic a laser passes a beam splitter. One beam is conducted through the plasma and then recombined with the other beam in a Mach-Zehnder interferometer. This

process is used along five different channels and the differences in phase shift are used to reproduce the line integrals of the density.[7] While DCN is the base data, DCK provides the line integrals corrected for fringe jumps and is therefore used if available.

ECE measures the electron cyclotron emission of the plasma. The electrons perform in a magnetic field a rotation around the magnetic axis of which the frequency only depends on the strength of the magnetic field. The diagnostic CEC measures the X-mode radiation of the 2nd harmonic of this gyration with a fast 60-channel heterodyne radiometer. The frequency depends on the magnetic field and therefore the radial position and the plasma is optically thick at the resonance, but optically thin for this frequency further outside. The power in each spectral region can therefore be mapped to the region of the resonance in the plasma and is proportional to the electron temperature at that location. [8]

TORBEAM is a paraxial WKB code for the description of electron cyclotron waves in fusion plasmas. This code takes the input data of the specific shot and then derives an absorption (and therefore heating profile) for the plasma. [9]

2.2 ASTRA

The simulation of the behavior of plasmas is a complex matter that is limited by the availability of data and computational resources. The ASTRA (Automatic System for TRansport Analysis) code is a programming system that integrates different sub-models into one executable model and allows easy use, update and interchange of the models.

ASTRA does this by providing a modular setup in which it plays the role of a tool that assembles a customized code according to the specifications of the end-user and then provides an interface for the viewer to interact with the execution.

Further information on this model can be found in [10].

2.3 TGLF

TGLF is the abbreviation for trapped-gyro-Landau-fluid which is a theory based model of turbulent transport. The term 'theory based model' is here taken to mean that it is constructed from a theory rather than fitted to empirical data. TGLF is a submodule of ASTRA which is provided with the parameters of each position and offers its calculated results to the generalized simulation. This simulation has been used a lot and is considered to be fairly reliable. [11] [12] [13]

In the later part of this thesis TGLF is also used on a single input, without going through ASTRA, to compute the spectra of the turbulences. This usage is the same as in the actual simulation, the isolation however allows to better interpret the results.

The TGLF model solves for the linear Eigenmodes of trapped ion and electron modes (TIM / TEM), electron and ion temperature gradient modes (E and ITG) and electromagnetic kinetic ballooning modes.

The growth rates of the linear modes are found numerically and combined with a saturation rule that uses the quasilinear weights from TGLF to determine the energy and particle fluxes. These saturation rules are derived from nonlinear simulations with the gyrokinetic codes GKS and GYRO [14].

Further information can be found in [15]

3 Application

For this study two different experiments of ASDEX Upgrade were simulated, the first to learn how to work with both ASTRA and TGLF and the second on an experiment with only ECRH, allowing to simulate different heating profiles in this purely ECR-heated plasma.

3.1 Run 36072

To familiarize with the simulation the run #36072 was chosen. It is a simulation that was recently computed for a paper[16], allowing to compare the results and to spot appearing problems or mistakes of the setup more easily.

#36072 was run on 30.4.19 under the title "High-beta non-inductive scenario with ICRH". In several aspects it was more complicated than the later run as it used not only ECRH but also both NBI and ICRH. Those additional heating sources incorporate other measures that are not relevant in a purely ECR-heated scenario, for example the non-thermalized ions that NBI produces. To simplify the task a time period was chosen for the simulation in which the ICRH was not used and only ECRH and NBI are relevant.

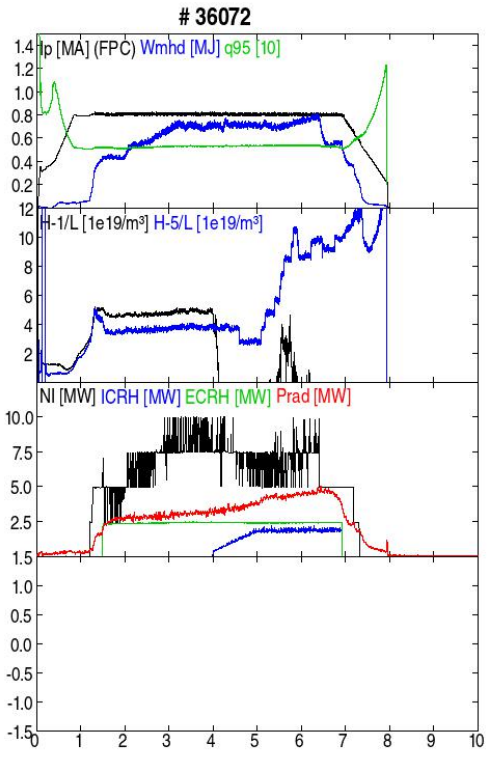

Figure 1: Control-room overview plot for #36072

ASTRA is using two input files, one containing experimental data and one the model, as explained in section 2.2. The model file was provided and the task was to recollect the experimental data an to cope with some changes to the ASTRA framework to assure the program chain gives

the same results.

The exp file specifies where to find the inputs as u-files. The basic structure of this exp file was generated by another program, trgui. In the basic file you have some of the parameters already available, for example the electron temperature, ion temperature and the electron density. It also contains some general information about the plasma, like the majority constituents (Z and mass), and the tokamak, including the minor radius, the chamber elongation, the chamber triangularity and the magnetic field.

The data for the temperatures and the density was taken out of the IDI (Ions) and IDA (electrons) diagnostics. These diagnostics are the Integrated Data Analysis (for Ion profiles) and combine several measurement diagnostics in a single set of data. The data used were the time averages over a period of 0.1s in which the plasma exhibits no significant changes.

Additional u-files for v_{tor} and μ (charge density) have been read out of the IDE and IDI shot-files by a python program.

The next u-files needed were concerning the NBI. Those were provided by the NUBEAM diagnostics. These files included the power deposition in electrons and in ions, the additional source of hydrogen particles due to the NBI and two u-files documenting the super-thermal ions (speed and pressure).

The data on the second heating mechanism, ECRH, was provided by another program, torbeam. [9]

Further information on the differing diagnostics can be found in section 2.1.

The model file assigned all the provided data to the variables that ASTRA is using. Additionally some other parameters like the effective charge, a measure for the concentration of non-hydrogen ions and therefore the impurity density, were specified here. The effective charge was set to 1.05 due to the high purity of the plasma. The ohmic heating is also considered in the heating power. The radiation losses were not provided but calculated by ASTRA from the differing constituents.

In the end the different submodules are linked to their corresponding variables (neoclassical, TGLF, etc.) and the temperatures are assigned to be updated every time step.

With these files assembled the actual simulation could be started.

The simulation for this run was mostly about preparing and extracting the data and less about the applicability of the model, so the simulation was run and found to be working. While the results were not perfect, the basis

was set for the actual setup to begin. They can be seen in fig. 2.

The resulting ion temperature was quite similar to the previous simulation with the electron profile actually being better, which is most likely due to this simulation using a newer version of TGLF.

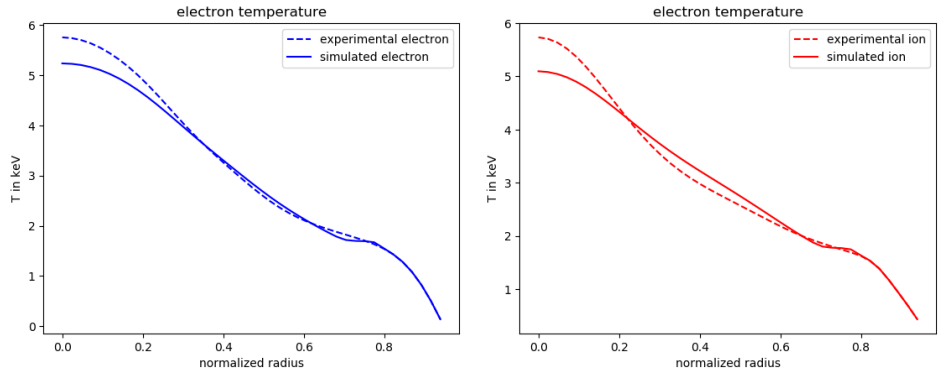

Figure 2: Temperatures of Electrons and Ions in comparison to the experimental value

3.2 Run 36222

The second simulation was of the run #36222. The experiment was run on 14.05.19. It can be used because it is one in a group of experiments which are only using ECRH and are in a collisionality regime in which the ion temperature diverges from the electron temperature in the center but converges closer to the boundary. This allows to change the electron temperature and evaluate the changing ion temperature while keeping the boundary condition at the pedestal top constant. Among these similar experiments 36222 was chosen as it shows a stable plasma at a time around 5s, which is when the NBI was turned on for a short time which gives us reliable results for the ion temperature.

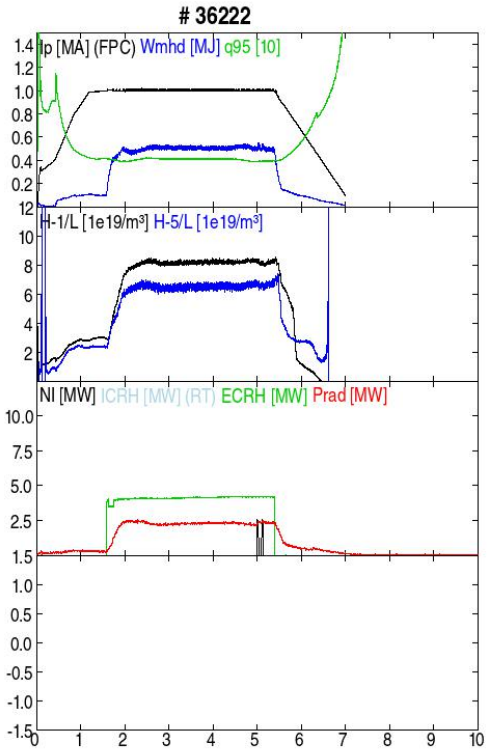

Figure 3: Control-room overview plot for #36222

Here the time interval from 4.9s to 5.0s was chosen for a simulation as reliable data on the plasma are available in that time frame and earlier time windows being not as convenient due to a vertical shift of the plasma around half a second earlier and the disturbances of the NBI at the later points of time.

The u-files were similar to the previous simulation, but the ones concerning the NBI were not needed and therefore omitted.

This only ECR-heated experiment exhibited a behavior that was not present in the previous simulation, the electron temperature fell and rose in a sawtooth form. This behavior has been modeled in previous simulations [17], but we substituted a constant in the electron heat capacity instead. The radial range of this constant increase was chosen to resemble the inversion radius of the sawtooth, while its height was adjusted to fit the temperature

curves.

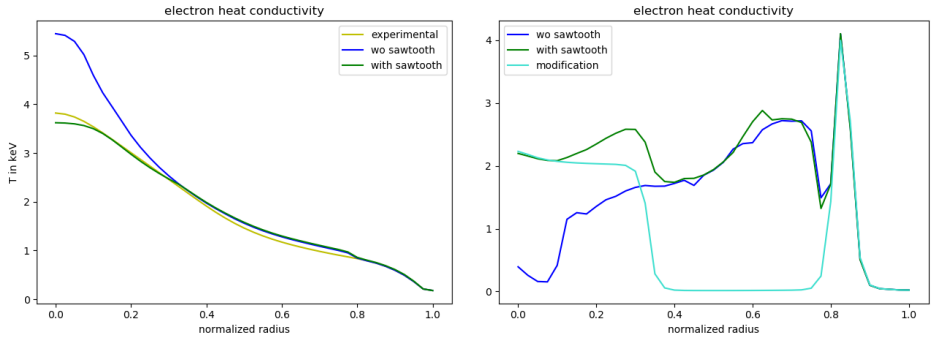

Figure 4: Electron temperature and heat conductivity before and after the application of the sawtooth model in comparison to the experimental value

Another problem that appeared was a step directly after the boundary in both ion and electron temperature. The same behavior has been observed in several other simulations.[18] This is known to be an artefact of the actual TGLF version. We used a workaround, adding a Gaussian modification to the heat conductivity of both electrons and ions at the boundary.

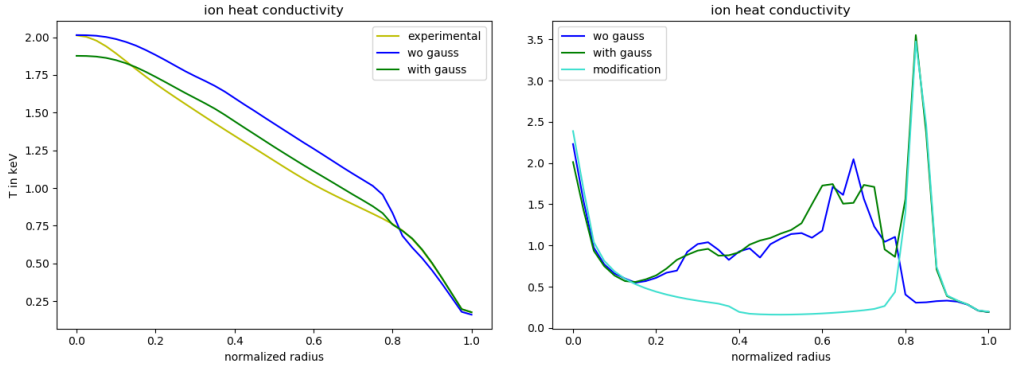

Figure 5: Ion temperature and heat conductivity before and after application of the gauss and the experimental value

The final simulation appears to predict the actual behavior of the plasma quite closely, which is why we used this version of the model to simulate variations of the ECR heating profile. The figures 6 and 5 show the radial

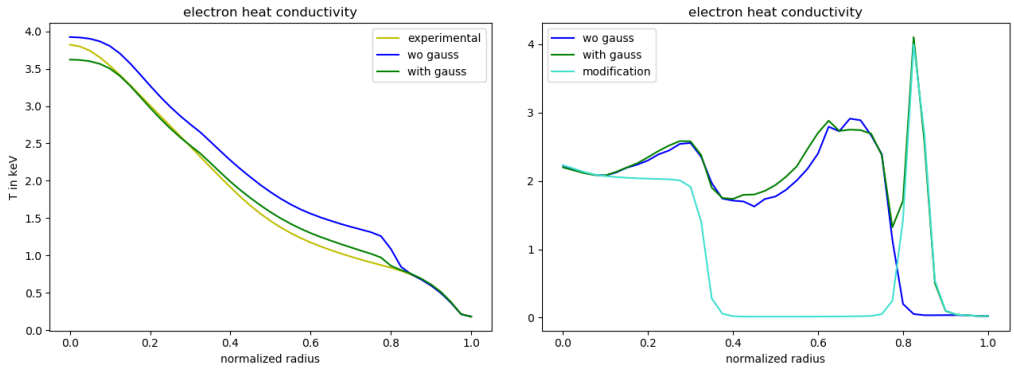

Figure 6: Electron temperature and heat conductivity before and after the application of the Gaussian

range in which the TGLF code dominates the transport and can therefore be used to achieve information on the different channels.

For ions these plots suggest that the model is reliable inside a radius of 0.75 while for the electrons this region is limited on the one hand by the plateau for the sawtooth model and on the other by the Gaussian on the boundary, so at radial positions between 0.35 and 0.7.

A possible source of errors in the used model is the fact that the model used a low value for Zeff (1.05) instead of the more realistic higher experimental value of around 1.8. Unfortunately this discrepancy was spotted only after the fact and could lead to differing results in experiments.

An additional problem with the model was the fact that it holds ne constant which can lead to contributions of turbulence due to electron flux.

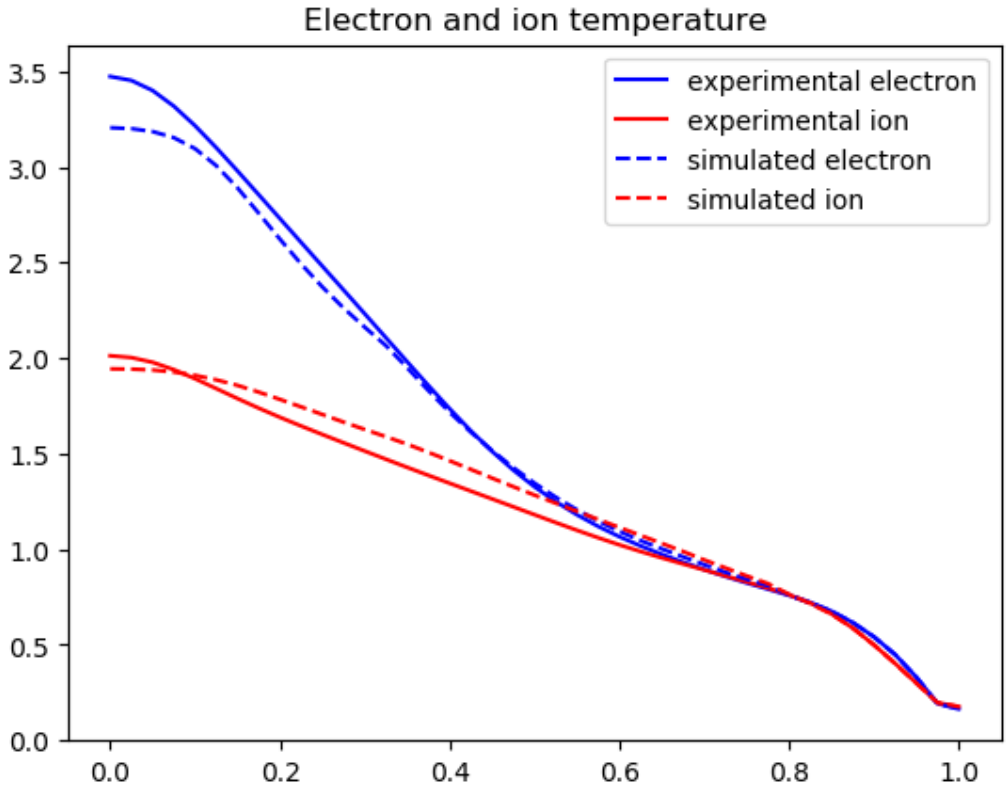

Figure 7: Ion and electron temperatures in the final simulation and the experiment

4 Modeling of the off-axis EC heating

4.1 General model

The aim of the simulation was to predict what would happen if an increasing percentage of the heating power was deposited not in the center but off-axis closer to the boundary.

To simulate this heating profile a Gaussian was placed close to the boundary, with the center at 0.7 (for comparison, the boundary is located at 0.8) and a width of 0.03 in the normalized minor radius. For each simulation the fraction of the power deposited in the Gaussian was increased while reducing the height of the original deposition profile, keeping the total ECR heating

constant

For this thesis 5 different fractions were modeled, moving from 100 % in the center, passing over 75, 50 and 25 %, to no power deposition in the center and complete deposition in the Gaussian.

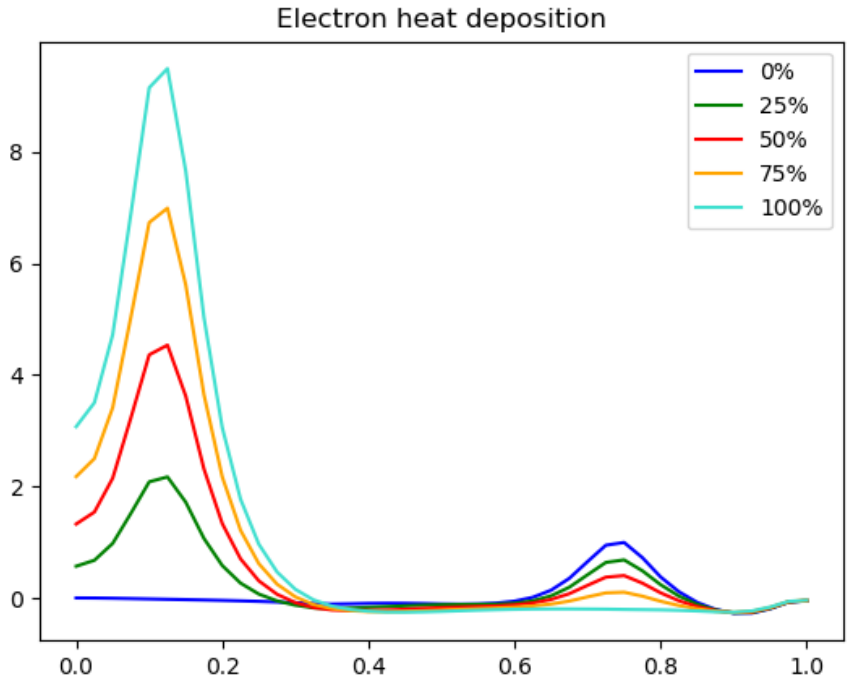

All 5 simulations were run from 4.9 s to 5.0 s and then evaluated. The results are shown in the following graphics. The modifications to the model (the sawtooth substitution and the additional conductivity at the boundary to remove the step) discussed in the previous subsection are also shown again for convenience.

Comparing the change of the core temperatures in Fig. 8 it is noticeable that the electron temperature changes significantly with the amount of heat deposited in the center and is practically flat if the entire heat is deposited next to the boundary. The differences between the core temperatures are almost equidistant for the different simulations.

The ion temperature however exhibits a different behavior: the general

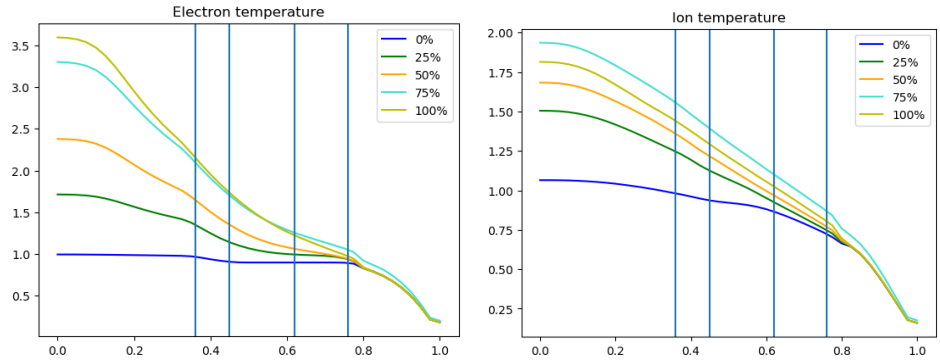

Figure 8: Temperature profiles of electrons and ions of the simulations in comparison to the experimental values

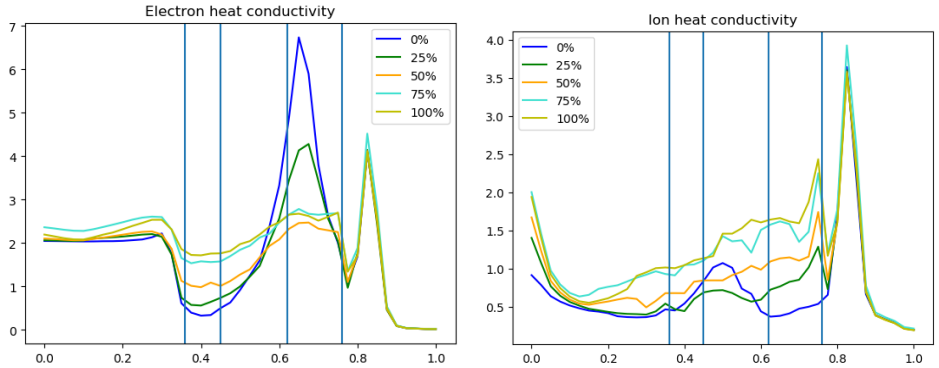

Figure 9: Heat conductivity profiles of electrons and ions of the simulations in comparison to the experimental values

shape remains closer to the case of 100 % central heating than for the electron temperature. Furthermore the core temperature does not change in equidistant steps like the electrons but rather remains closely aligned for 50 % to 100 %, it even increases as you modify the central heating from 100 to 75%. It only begins to change significantly with the 25 % case. The largest reduction is observed for the step from 25% to 0%.

The heat flux seems like one would expect (for all cases except the 0% central deposition) with it strongly peaking in the electrons in the center at the heat deposition, decreasing the further you get outside and peaking again at the outer heat deposition. The ion heat flux steadily increases. The

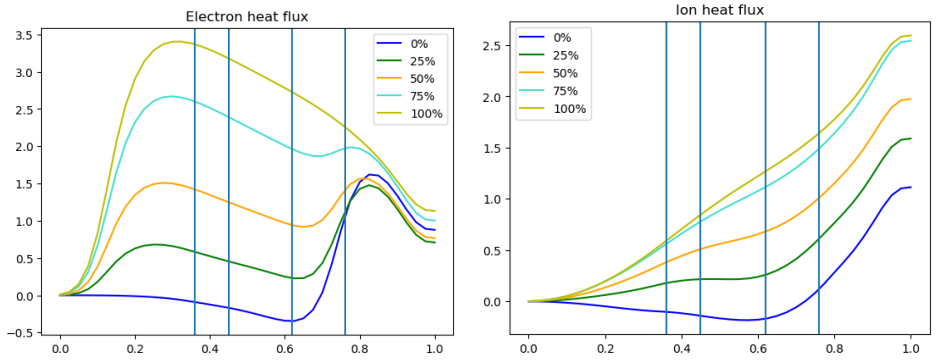

Figure 10: Heat flux profiles of electrons and ions of the simulations in comparison to the experimental values

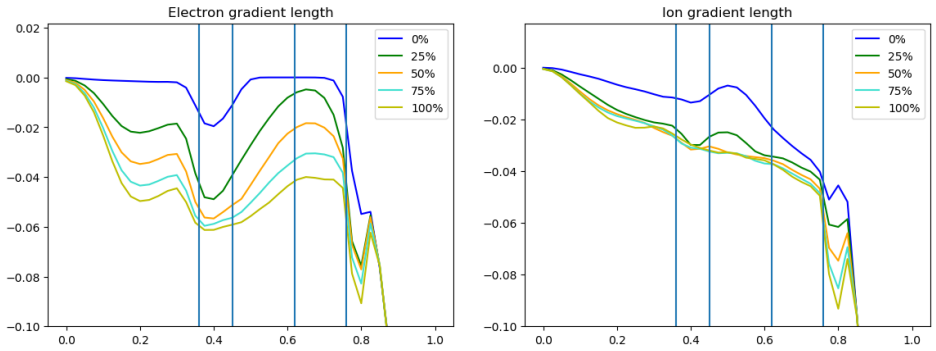

Figure 11: gradient length of the temperture curves

exception is the 0% case in which the is even a negative heat flux. This compares to the very flat profile in both electrons and ions. Note, that the sawtooth parameters are unchanged, which may be unphysical and a potential cause for the negative heat flux.

In fig. 11 the gradient length (ratio of the temperature gradient and the temperature) is plotted. For the electrons the inverse gradient length decreases between the sawtooth inversion radius and the outer heat source as the inner heat source is decreased.

For the inverse ion gradient length the curves are nearly identical for all simulations with non-zero central heating. Such strong similarities correspond to a very stiff temperature curve, similar to the expectations. Differing from the electrons the ion gradient length also changes only very slowly with

the radius.

This suggests that a large portion of the central heating can be removed and transferred to the off-axis region before a major effect on the ion temperature can be observed.

4.2 Spectra

The next step used TGLF to generate spectra which map the heat flux against the turbulence size. Along with the correlating frequency of the turbulence these spectra can be used to analyze how the differing turbulence modes contribute to the transport either at the same position and differing heating or for the same central heating and changing radial position.

In the next section a closer look onto how the spectra were generated is offered.

The spectra plot the integrated spectral heat flux in each species or the frequency of turbulence modes against their wave number. The inverse of the wave number is a measure of the size of the disturbance and can be used to estimate the species of turbulence. The integral of the spectral heat flux was chosen because it allows to interpret the contributions to the total regardless of the logarithmic scale of the steps in the wave number.

k_y is normalized in the sound-gyro-radius ($\sqrt{\frac{T_e}{m_i}}\frac{1}{f*a}n_e T_e * S$, where a is the minor radius, S is the surface and f is the ion cyclotron frequency), which means that values of larger than 1 have to be electron modes while the lower values can also be ion modes, primarily the ion temperature gradient (ITG). The electron modes can be either the electron temperature gradient (ETG) or the trapped electron mode (TEM). The TEM may contribute at two length scales: large scale TEMs for k_y well below 1 and small scale TEMs for k_y above unity. They can be distinguished from the ITG by the rotational frequency which is negative for ions and positive for electrons (according to their charge). A rapid increase of the rotational frequency for k_y just below 10 indicates that ETGs become dominant for those scales.

The normalization of the k_y impacts also the total values of the integrated fluxes, which is why to get a better feeling for the total magnitude the absolute values of the fluxes in MW are additionally given in tables while the graphics contain the uncorrected values.

4 different radial positions were evaluated. The first position is at a normalized radius of 0.36. Data from further inside is not reliable as the

sawtooth substitution model artificially changes the transport here. The next step is further outside at 0.45, in the middle between the outer and the inner deposition. The third position was chosen a short distance in front of the outer heat deposition, at 0.62, while the last one is between the outer heat deposition and the additional Gaussian that removes the step at the boundary at 0.76.

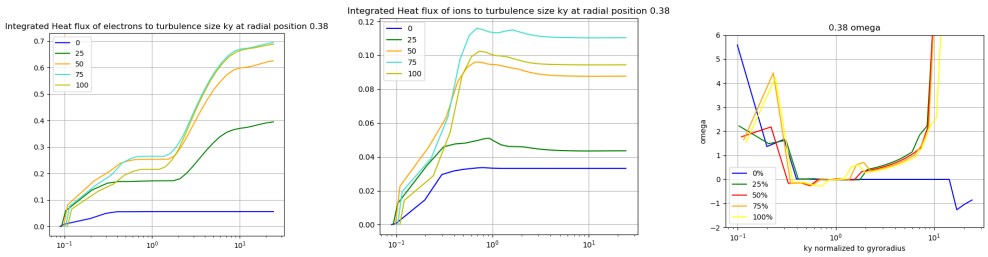

Figure 12: Integrated Heat flux and frequency at radius 0.38

The integrated heat flux (separately for electrons and ions) and the frequency omega can be seen in Fig. 12 for the first position, i.e. a normalized radius of 0.38. The total contributions are shown in 13.

At this position we have for the centrally heated scenarios for the electrons a contribution of low and large k_y TEM. The rotational frequency indicates that for the highest k_y ETGs set in, but their contribution to the total heat flux in the electron channel is below 10 %. Ion transport is dominated by ITG modes around the sound radius and by large scale TEMs or sub-dominant ITGs for smaller k_y.

The graphs especially for the highest centrally heated scenarios all look very similar in both flux and frequency, with only the lowest centrally heated scenarios exhibiting markedly different behavior in the sense that the contribution of small scale TEMs and ITGs is reduced.

Power deposition in center in %	0	25	50	75	100
Energy flux through the electrons in MW	0.245	1.023	2.34	3.38	3.98
Energy flux trough the ions in MW	0.175	0.113	0.329	0.519	0.635

Figure 13: Energy fluxes of the different simulation at radius 0.36

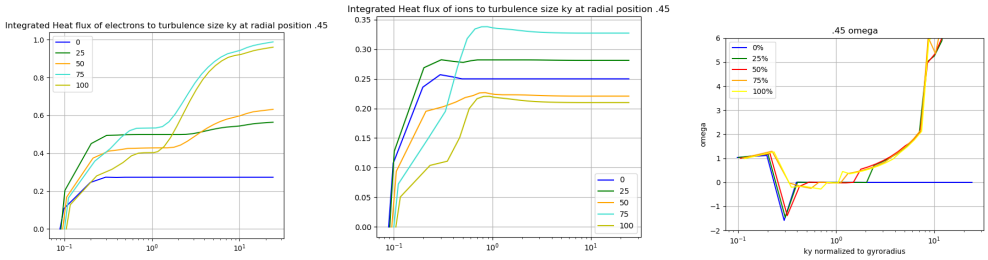

Figure 14: Integrated Heat flux and frequency at radius 0.45

Power deposition in center in %	0	25	50	75	100
Energy flux through the electrons in MW	0.326	1.017	1.638	3.159	4.406
Energy flux trough the ions in MW	0.289	0.495	0.641	0.877	0.979

Figure 15: Energy fluxes of the different simulation at radius 0.45

The next spectrum (14) was taken at the radial position of 0.45 in the middle of the two heat deposition sites. The total heat transport values can be seen in 15.

At this position the behavior for 100% and 75% central heating is qualitatively similar to the previous case, but for 50% and 25% the small scale TEM is almost absent since electron and ion temperature are approaching each other. Under these conditions ETGs do contribute almost 30 % of the electron heat transport (in the case of 50% central heating). Ion transport at this position is still dominated at very low k_y by TEM or a sub-dominant ITG, only for the more centrally heated cases a substantial contribution of dominant ITG to the heat flux is visible.

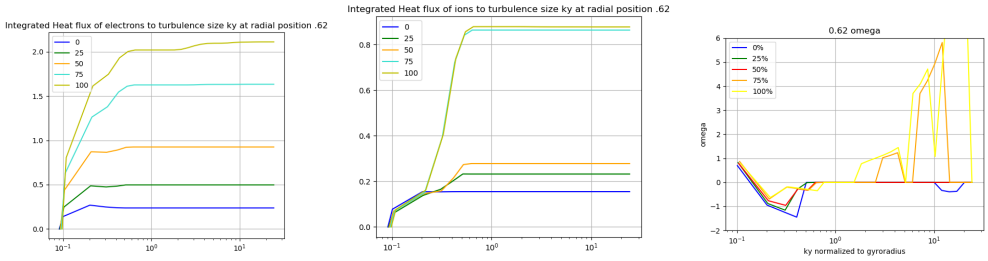

Figure 16: Integrated Heat flux and frequency at radius 0.62

Power deposition in center in %	0	25	50	75	100
Energy flux through the electrons in MW	0.323	1.017	1.638	2.424	3.615
Energy flux trough the ions in MW	0.290	0.495	0.641	1.312	1.475

Figure 17: Energy fluxes of the different simulation at radius 0.62

The next spectra 16 are taken shortly before the outer heat deposition. In 17 the total values can be found.

The development from the previous spectra has continued, with high k_y modes having almost vanished.

As before the contribution of the ITG modes is important for both channels for central heating, while the remainder is generated from large scale TEM modes. The majority of the flux is however still through the electrons.

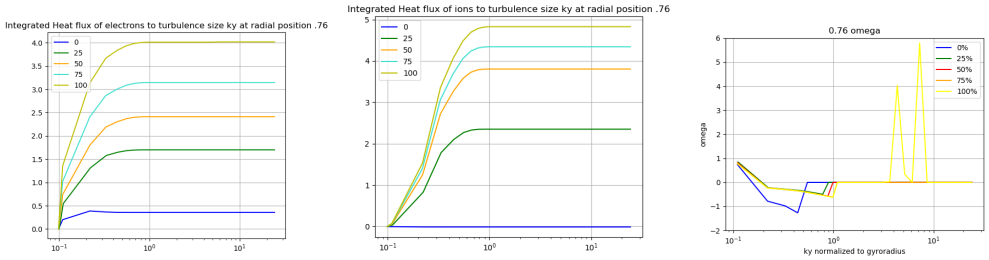

Figure 18: Integrated Heat flux and frequency at radius 0.76

Power deposition in center in %	0	25	50	75	100
Energy flux through the electrons in MW	4.204	2.369	2.044	2.211	2.298
Energy flux trough the ions in MW	0.513	3.207	3.255	3.010	3.154

Figure 19: Energy fluxes of the different simulation at radius 0.76

As similar behavior is also seen at the spectrum the furthest outside. Here the dominant mode is the ITG, with contributions of the low k_y TEM. The flux through electrons and ions has almost equalized /inverted for the centrally heated.

The next spectra show contour plots of the quantities for one scenario each in a diagram of ky and radius. The integrated heat flux spectra are separately normalized to unity at the boundary to allow to separate the contributions of the different modes. Two additional positions were computed for this, 0.515 and 0.58.

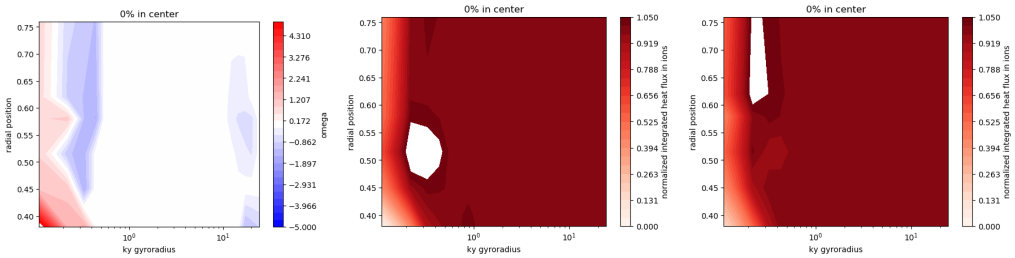

Figure 20: Contourplots of normalized heat flux and frequency for 0% central heating

The first contour plot 20 show the scenario with no central heating. All the significant transport occurs at low k_y.

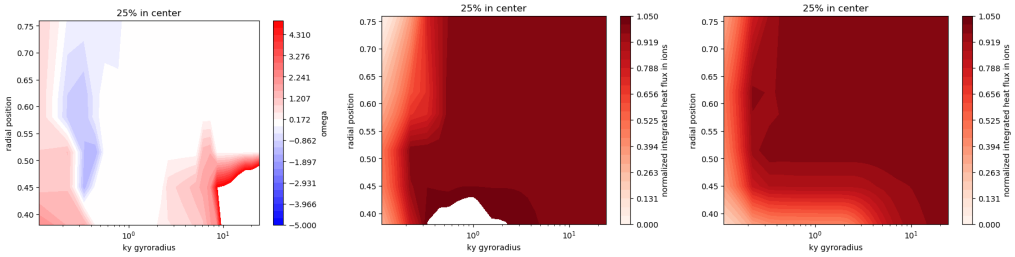

Figure 21: Contourplots of normalized heat flux and frequency for 25% central heating

In the second plot 21 25 % of the heat deposition occurs in the center. Here the main transport occurs near the core in the small scale TEM mode but moves very quickly to the low k_y modes, where an ITG mode increases in importance the further outside we get.

A similar scenario occurs in 22 with the change from high k_y modes occurring further outside and the ITG mode not being as dominant (with high negative frequency).

The plots for the two highest heating fractions, 23 and 24 again show a very similar behavior to each other, with both of them having a significant

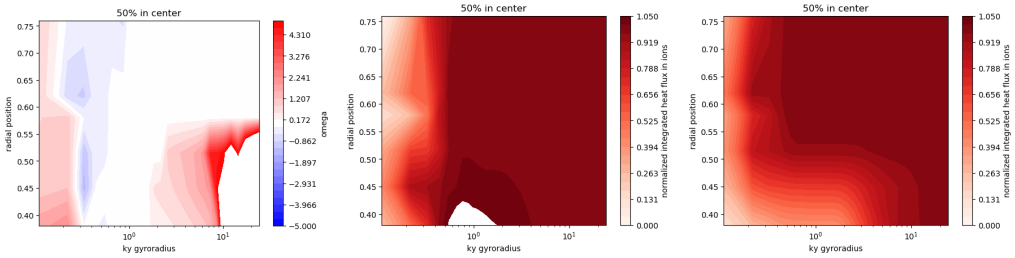

Figure 22: Contourplots of normalized heat flux and frequency for 50% central heating

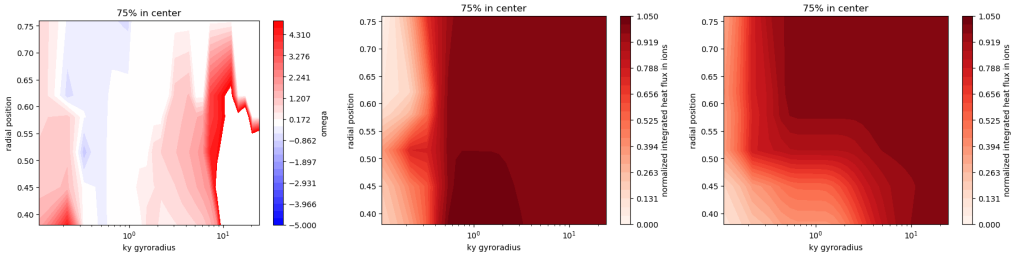

Figure 23: Contourplots of normalized heat flux and frequency for 75% central heating

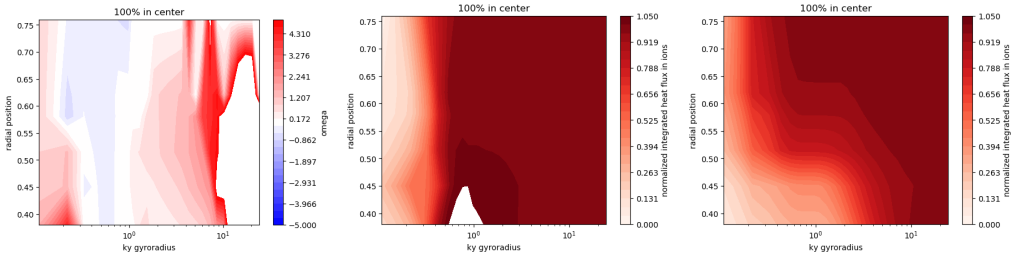

Figure 24: Contour plots of normalized heat flux and frequency for 100% central heating

high k_y contribution for relatively long and an increasing ITG mode that is however not completely dominating in the frequencies.

4.3 Plots

This report uses several different Plots to show and in this section the differing methods to create them are described:

The plots for the time traces (Figs. 3.1, 3.2) were not created by me, but rather taken from the IPP Intranet.

For the radial profiles (Figures 2, 4, 5, 6, 3.2, 4.1, 8, 10, 11) the data was provided by the ASTRA Simulation and from that written into UFILES, an ASCII format the definition of which can be found here:

http://w3.pppl.gov/ pshare/help/ufiles_manual.html .

A programm orginally from Emiliano Fable was used to extract the data from those files and plotted it in python.

The data for the wavelength spectra (Figures 12 14, 16, 18) was extracted by the standalone tglf. For that it is necessary to take from the /xpr/ file of our astra directory the tglfin_* File which corresponds to corresponds to your wanted radial position (the radial position is written in the file itself) and transfer it to the standalone directory, where the xtglf is then run. This then creates four different files starting with fort. The one needed for my spectra is fort.887 which contains in the first column the wavelengths ky and in the 6th and 7th column the spectral density of the electron and ion heat flux. The fort.887 file is an ASCII file with the columns seperated by whitespaces. After reading it from the file it is necessary to convert it to a number.

After obtaining the numerical values for the kys and the fluxes it is possible to generate the spectras. To generate the integrated fluxes the averages of the current and previous spectral density is multiplied with the length of the step between the current and previous value of ky, added onto the previous values and appended to a list. This list is then plottat against the list of the kys.

The countour plots (Figures 20 21, 22, 23, 24) are generated analogously by stacking plots of different radial positions.

5 Conclusions

Similar to observations in [3] the TGLF simulation predicts that changes in the fraction of the central heat deposition affect the electron temperatures very little. Even changes of 25% produce only marginal results, to see a real change in the core temperature, more than 50% have to be removed.

The small scale TEM modes are only very relevant just outside the EC deposition, otherwise the ITG and long scale TEM modes play the major role. As long as the ratio of electron to ion temperature is not too high and the heat flux is substantial, the major contributor is the ITG.

There were a few substitutions in my simulation that could, if corrected, change my results: The substitution we chose for the sawtooth transport, replacing it with a constant pedestal in the center, is not a very reliable model. For the changing core temperatures the frequency of the sawtooth could change (most likely decrease), which would affect the height of the pedestal, its radius could change or at some point it could even stop. These circumstances are not considered in the model. This however should not be too much of a problem as it almost only affects the electron temperature. An additional Problem was that my simulation held the electron density constant which lead to strange behaviors in the unheated case.

Another problem could occur due to the workaround at the boundary, this should however still not be too much of a problem as all my calculations are outside of the artificially changed region.

My suggestion for future experiments would be to move a large fraction, maybe up to 50% of the ECR-heating should be moved off-axis, then the actual effect on the ion temperature could be compared to the prediction.

Another topic for research could also be to model how much NBI would be needed to affect a major change in the ion core temperature and how the NBI would have to be configured.

6 Bibliography

References

[1] T.H. Stix. Heating of toroidal plasmas by neutral injection. *Plasma Physics*, 14(367), 1972.

[2] H.P. Laqua et al. Overview of w7-x results. *EPJ Web Conf.*, 203(02002), 2019.

[3] O. Ford et al. Ion temperature profiles in nbi and ecrh heated wendelstein 7-x plasmas.

[4] S.A. Bozhenkov et al. High performance pellet experiments in wendelstein 7-x. submitted 2019.

[5] R.Fischer et al. Bayesian modelling of fusion diagnostics. *Plasma Physics and Controlled Fusion*, 45(7), 2003.

[6] Dux Viezzer, Puetterich and Dermott. High-resolution charge exchange measurements at asdex-upgrade. *Rev Sci Intrum*, 83(103501), 2012.

[7] A. Mlynek et al. Fringe jump analysis and implementation of polarimetry on the asdex upgrade dcn interferometer. *Review of Scientific Instruments*, 85, 2014.

[8] Denk et al. Analysis of electron cyclotron emission with extended electron cuclotron forward modeling. *Plasma Physics and Controlled Fusion*, 60, 2018.

[9] E.Poli et al. Torbeam 2.0, a paraxial beam tracing code for electron-cyclotron beams in fusion plasmas for extended physics applications. *Computer Physics Communication*, 225, 2018.

[10] E. Fable (addendum for 7.0) G.V. Perverzev, P.N. Yushmanov. *ASTRA Automated System for TRansport Analysis*. 2002 (addendum 2012).

[11] Waltz Kinsey, Staebler. The first transport code simulations using the trapped gyro-landau-fluid model. *Phsyics of Plasmas*, 15(055908), 2008.

[12] C.Pan et al. Investigation of energy transport in diii-d high-? p east-demonstration discharges with the tglf turbulent and neo neoclassical transport models. *Nuclear Fusion*, 57, 2017.

[13] B. Baiocchi et al. Turbulent transport analysis of jet h-mode and hybrid plasmas using qualikiz and trapped gyro landau fluid. *Plasma Physics and Controlled Fusion*, 57(3), 2015.

[14] R.E.Waltz J.Candy. An eulerian gyrokinetic-maxwell solver. *Journal of Computational Physics*, 186, 2003.

[15] Waltz Staebler, Kinsey. Gyro landau fluid equations for trapped and passing particles. *Phys. Plasmas*, 12(102508), 2005.

[16] M. Reisner et al. Increased core ion temperatures in high beta advanced scenarios in asdex upgrade. *Nuclear Fusion*, submitted 2019.

[17] F. Ryter et al. Heat transport driven by the ion temperature gradient and electron temperature gradient instabilities in asdex upgrade h-modes. *Nucl. Fusion*, 59(096052), 2019.

[18] Kinsey et al. Predictions of the near edge transport shortfall in diii-d l-mode plasmas using the trapped gyro-landau-fluid model. *Pysics of Plasmas*, 22(012507), 2015.

7 Acknowledgments

I would like to thank Joerg Stober for providing me with this subject, the necessary research materials and advice in every stage of the work.

Maximilian Reisner gave me an introduction into the used programms as well as access to his tools and programs for the preparation of the data and the results..

Further I want to thank Emiliano Fable for his help with the simulation and the interpretation of the results.

Giovanni Tardini helped with any occuring problems and bugs in the software.